

Constraints from Triple Gauge Couplings on Vectorlike Leptons

Enrico Bertuzzo,^a Pedro A. N. Machado,^b Yuber F. Perez-Gonzalez,^a Renata Zukanovich Funchal^a

^a*Departamento de Física Matemática, Instituto de Física, Universidade de São Paulo, Rua do Matão 1371, CEP. 05508-090, São Paulo, Brazil*

^b*Fermi National Accelerator Laboratory, Batavia, IL, 60510, USA*

E-mail: bertuzzo@if.usp.br, pmachado@fnal.gov, yfperezg@if.usp.br, zukanov@if.usp.br

ABSTRACT: We study the contributions of colorless vectorlike fermions to the triple gauge couplings $W^+W^-\gamma$ and $W^+W^-Z^0$. We consider models in which their coupling to the Standard Model Higgs boson is allowed or forbidden by quantum numbers. We assess the sensitivity of the future accelerators FCC-ee, ILC and CLIC to the parameters of these models, assuming they will be able to constrain the anomalous triple gauge couplings with a precision $\delta\kappa_V \sim \mathcal{O}(10^{-4})$, $V = \gamma, Z^0$. We show that the combination of measurements at different center-of-mass energies helps to improve the sensitivity to the contribution of vectorlike fermions, in particular when they couple to the Higgs. In fact, the measurements at the FCC-ee and, especially, the ILC and the CLIC, may turn the triple gauge couplings into a new set of precision parameters able to constrain the models better than the oblique parameters or the $H \rightarrow \gamma\gamma$ decay, even assuming the considerable improvement of the latter measurements achievable at the new machines.

Published in *Phys. Rev. D*

Contents

1	Introduction	1
2	Triple gauge couplings	2
3	Models of colorless vectorlike fermions	4
3.1	Unmixed colorless vectorlike fermions	4
3.2	Mixed colorless vectorlike fermions	6
4	TGC constraints on vectorlike colorless fermion models	9
5	Conclusions	13
A	Vectorlike fermion contribution to triple gauge couplings	16
B	Dependence on the hypercharge in the unmixed case	17

1 Introduction

All experimental data collected so far have confirmed the Standard Model (SM) predictions, including the existence of a scalar particle that seems to have the right properties to match those of a Higgs boson. The SM cannot, however, be the final theory of particle physics, since it does not explain neutrino masses nor the baryon asymmetry of the Universe and it does not contain a dark matter (DM) candidate. Moreover, if the naturalness principle applies, new physics (NP) is expected.

The nature of the NP models that are supposed to complete the SM is elusive and unknown. Taking a bottom-up approach, however, we can suppose that, exactly as the SM particles are vectorlike from the low-energy QED/QCD point of view, the first particles to be discovered (if any) will be vectorlike from the SM point of view [1]. In addition, vectorlike fermions arise in many well-motivated SM extensions such as models with extra dimensions [2–5], composite Higgs [6–8], two-Higgs-doublet-model extensions [9], low-scale supersymmetry [10, 11] and, more recently, in new solutions of the hierarchy problem [12, 13]. Vectorlike fermions are much less constrained than extra chiral families, which in fact are now pretty much ruled out by data after the observation of the 125 GeV boson at the LHC [14, 15]. Vectorlike quarks masses are typically bounded from ATLAS and CMS Run 1 data to be $\gtrsim (800\text{--}1000)$ GeV [16–23], while direct constraints on vectorlike leptons come only from the LEP experiments and are constrained to be $\gtrsim 100$ GeV [24]. Bounds

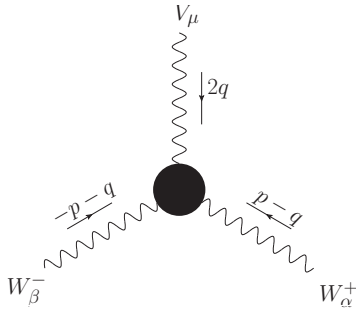


Figure 1. Feynman diagram of the WWV vertex in momentum space.

from electric and magnetic dipole moments and electroweak precision measurements have been also considered [25, 26].

As no new particles have been discovered so far, there is growing interest in the community in future $e^+ e^-$ colliders that could pursue the electroweak precision tests started by LEP and the SLC profiting of higher energies and luminosities. This moves from the observation that, for heavy enough particles, NP may first show up through loop effects, and as such be bounded by electroweak precision measurements, modifications of $H \rightarrow \gamma\gamma$ or anomalous triple gauge couplings (TGCs). In particular, the new machines can probe the anomalous TGCs $W^+W^-\gamma$, $W^+W^-Z^0$, and $Z^0Z^0\gamma$ to unprecedented levels. Since the structure of the TGCs is a direct manifestation of the non-Abelian nature of the SM gauge group, they are sensitive to the presence of NP with $SU(2)_L \times U(1)_Y$ representation and, in particular, to the presence of vectorlike fermions.

The purpose of this paper is to estimate the sensitivity of future $e^+ e^-$ machines to vectorlike leptons, in many possible realizations, via the measurements of triple gauge couplings which will putatively reach a $\mathcal{O}(10^{-4})$ precision. The paper is organized as follows. In Sec. 2 we start by defining the TGCs form factors that can be modified by SM loop corrections and new physics. Next, in Sec. 3 we describe the vectorlike lepton models that we will study in this paper and how they can contribute to the TGCs form factors. In Sec. 4 we estimate the constraints on these models that can be achieved by TGCs measurements at three proposed future accelerator facilities: the Future Circular Collider (FCC-ee) [27], International Linear Collider (ILC) [28], and the Compact Linear Collider (CLIC) [29]. Finally, in Sec. 5, we discuss our conclusions.

2 Triple gauge couplings

The typical structure of the charged TGCs that we will consider in this paper is shown in Fig. 1, where V can be either the Z^0 boson or the photon. The complete one-loop SM contribution to the charged TGCs $W^+W^-\gamma$ and $W^+W^-Z^0$ was computed some time ago [30–32], while the contribution to the neutral TGC $Z^0Z^0\gamma$ was studied in Refs. [30, 33]. The charged couplings can be directly studied in future e^+e^- colliders, through $e^+e^- \rightarrow$

W^+W^- . The neutral couplings, on the other hand, can be studied using the processes $e^+e^- \rightarrow Z^0\gamma$ or $e^+e^- \rightarrow Z^0Z^0$, with subsequent decays $Z^0 \rightarrow \bar{\nu}\nu$ and $Z^0 \rightarrow \ell^+\ell^-$ [34–36]. Let us note that only fermions with an axial coupling to the Z^0 boson can generate nonvanishing corrections to the neutral TGCs [33]. As such, since our focus is vectorlike fermions, we will just consider the effects on the charged vertices.

The generic charged TGC vertex WWV , with $V = \gamma, Z^0$, can be parametrized using the effective Lagrangian [37]

$$\begin{aligned} \mathcal{L}_{WWV} = & -ig_V[(W_{\mu\nu}^\dagger W^\mu V^\nu - W_{\mu\nu} W^{\mu\dagger} V^\nu) + \kappa_V W_\mu^\dagger W_\nu V^{\mu\nu} + \frac{\lambda_V}{M_W^2} W_{\mu\tau}^\dagger W_\nu^\tau V^{\nu\mu} \\ & + \mathcal{L}_{WWV}^{\text{nCP}}, \end{aligned} \quad (2.1)$$

where $\mathcal{L}_{WWV}^{\text{nCP}}$ contains P or C odd terms, κ_V and λ_V are form factors, the field strengths are defined as $W_{\mu\nu} = \partial_\mu W_\nu - \partial_\nu W_\mu$ ¹ and $V_{\mu\nu} = \partial_\mu V_\nu - \partial_\nu V_\mu$, and the coupling g_V is given by

$$g_V = \begin{cases} e & \text{for } V = \gamma, \\ e \cot \theta_W & \text{for } V = Z^0. \end{cases} \quad (2.2)$$

In the SM at tree level, $\kappa_V = 1$ and $\lambda_V = 0$. We will focus only on the C - and P -conserving terms, discarding $\mathcal{L}_{WWV}^{\text{nCP}}$ in the following. In the photon case, the form factors are related to the static properties of the W boson (namely the magnetic dipole μ_W and the electric quadrupole moment Q_W) through the relations [37]

$$\begin{aligned} \mu_W &= \frac{e}{2M_W}(1 + \kappa_\gamma + \lambda_\gamma), \\ Q_W &= -\frac{e}{M_W^2}(\kappa_\gamma - \lambda_\gamma). \end{aligned} \quad (2.3)$$

Following a notation analogous to the one used in Ref. [30] (see Fig. 1 for the definition of the momenta), the WWV vertex in momentum space can be written as

$$\begin{aligned} \Gamma_{\mu\alpha\beta}^V = & -ig_V \left\{ f(q^2) [2g_{\alpha\beta} p_\mu + 4(g_{\alpha\mu} q_\beta - g_{\beta\mu} q_\alpha)] + 2\Delta\kappa_V(q^2)(g_{\alpha\mu} q_\beta - g_{\beta\mu} q_\alpha) \right. \\ & \left. + 4\frac{\Delta Q_V(q^2)}{M_W^2} \left(p_\mu q_\alpha q_\beta - \frac{1}{2}q^2 g_{\alpha\beta} p_\mu \right) \right\}, \end{aligned} \quad (2.4)$$

with the $f(q^2)$ form factor connected to the renormalization of the charge, while $\Delta\kappa_V(q^2)$ and $\Delta Q_V(q^2)$, related to κ_V and λ_V through the expressions

$$\begin{aligned} \Delta\kappa_V &= \kappa_V + \lambda_V - 1 \equiv \Delta\kappa_V^{SM} + \Delta\kappa_V^{NP}, \\ \Delta Q_V &= -2\lambda_V \equiv \Delta Q_V^{SM} + \Delta Q_V^{NP}, \end{aligned} \quad (2.5)$$

are designed to be zero at tree level in the SM. The SM one-loop contributions can be found in Refs. [30–32], while the explicit calculation of $\Delta\kappa_V^{NP}$ and ΔQ_V^{NP} in the case of vectorlike fermions is presented in Appendix A.

¹Notice that, with this definition, the W field strength is not $U(1)_{em}$ invariant. New quadrilinear terms must be introduced in \mathcal{L} to make the whole Lagrangian gauge invariant.

The quantity used by the experimental collaborations to show their results is the deviation from the SM value of κ_V at tree level, $\delta\kappa_V = \kappa_V - 1$, which will correspond to a linear combination of $\Delta\kappa_V$ and ΔQ_V , namely,

$$\delta\kappa_V = \Delta\kappa_V + \frac{1}{2}\Delta Q_V, \quad (2.6)$$

and this is the quantity we will be using throughout the paper.

3 Models of colorless vectorlike fermions

For our study, we will consider two classes of colorless vectorlike fermions: *(i)* a set of fermions in a unique $SU(2)_L$ representation, with no couplings to the Higgs boson allowed, and *(ii)* a set of at least two extra fermions in representations such that a Yukawa term with the Higgs boson is allowed. In both cases, we will assume that, due to some unspecified symmetry \mathcal{G} , all the mixing between the vectorlike and the SM fermions is forbidden.

3.1 Unmixed colorless vectorlike fermions

As already mentioned, we start adding to the SM particle content one vectorlike fermion Ψ , transforming under $SU(2)_L \times U(1)_Y$ as $\Psi \sim (\mathbf{2j} + \mathbf{1}, Y)$ and with mass m_Ψ . The Lagrangian is given by

$$\mathcal{L} = i\bar{\Psi}\gamma^\mu(\partial_\mu - igW_\mu^a T^a - ig'YB_\mu)\Psi - m_\Psi\bar{\Psi}\Psi, \quad (3.1)$$

where T^a are the $2j + 1$ -dimensional generators of the $SU(2)_L$ Lie algebra. An important consequence of considering a unique $SU(2)_L$ representation for all the N_F vectorlike fermions is that the $\delta\kappa_V^\Psi$ form factor just depends on the hypercharge and on the dimension j of the $SU(2)_L$ representation and not on the eigenvalues of the T^3 operator. This is shown explicitly in Appendix B, from which we see that we can write

$$\delta\kappa_V^\Psi \propto F_j I(m_\Psi), \quad F_j \equiv N_F Y \frac{2}{3} j(j+1)(2j+1), \quad (3.2)$$

where $I(m_\Psi)$ is a loop factor that only depends on the vectorlike lepton mass m_Ψ . An equivalent statement is that all the contributions to the $W^+W^-W^3$ TGC cancel out, leaving only W^+W^-B (with B the hypercharge gauge boson). Integrating numerically over the Feynman parameters of Eq. (A.1) we obtain $\Delta\kappa_V^\Psi$ and $\Delta\kappa_Z^\Psi$ as a function of $\sqrt{s} = \sqrt{(2q)^2}$ (see Appendix A for details).

In Fig. 2 we show the contour lines for $\delta\kappa_V^\Psi$ in the $(m_\Psi, |F_j|)$ plane for the four different center-of-mass energies $\sqrt{s} = m_H, 500 \text{ GeV}, 1 \text{ TeV},$ and 3 TeV . We observe that $|\delta\kappa_\gamma^\Psi| < |\delta\kappa_{Z^0}^\Psi|$ and they have opposite sign [see Eq. (B.12) in Appendix B]. The typical values of $|\delta\kappa_V^\Psi|$ are smaller than a few 10^{-4} .

For fixed \sqrt{s} , the loop factor in Eq. (3.2) vanishes for $m_\Psi = m_{\Psi_1}$ and $m_\Psi = m_{\Psi_2}$, where m_{Ψ_1, Ψ_2} are complicated functions of \sqrt{s} . The general behavior of $\delta\kappa_\gamma^\Psi$ as a function of

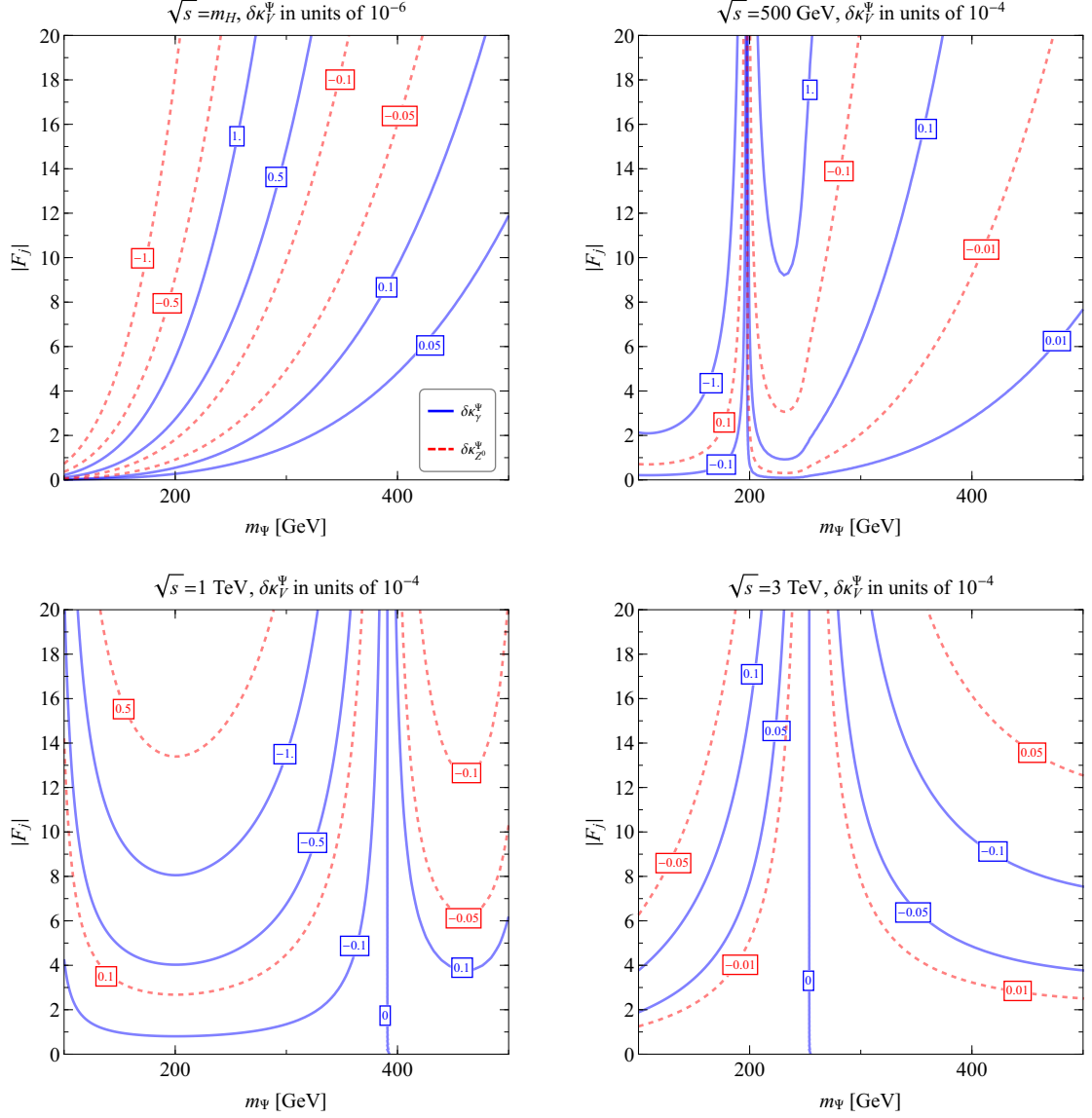


Figure 2. Contour lines of $\delta\kappa_V^\Psi$ [see Eq. (2.6)] in the plane $(m_\Psi, |F_j|)$ for the models with unmixed vectorlike colorless fermions (vectorlike leptons) at four different center-of-mass energies: $\sqrt{s} = m_H, 500 \text{ GeV}, 1 \text{ TeV},$ and 3 TeV . For the definition of F_j , see Eq. (3.2). The full blue (dashed red) lines correspond to $V = \gamma (Z^0)$.

m_Ψ is the following: it starts positive, vanishes for $m_\Psi = m_{\Psi_1}$, goes through a minimum (negative) value, increases again until it reaches zero for $m_\Psi = m_{\Psi_2}$, goes through a maximum (positive) value, and then decreases again until it goes back to zero. Because of the flip in sign, $\delta\kappa_{Z^0}^\Psi$ has the opposite behavior. For $\sqrt{s} = m_H$, both cancellations occur for $m_\Psi < 100 \text{ GeV}$, so they do not appear in the plot. For $\sqrt{s} = 500 \text{ GeV}$ and 1 TeV , we can only see in Fig. 2 the second cancellation at $m_{\Psi_2} \approx 200$ and 400 GeV , respectively, while for $\sqrt{s} = 3 \text{ TeV}$, we can see the first cancellation at $m_{\Psi_1} \approx 250 \text{ GeV}$. Note that after the second cancellation the loop integral gets suppressed (m_Ψ becomes too off shell for that

specific center-of-mass energy) so to reach the same $|\delta\kappa_V^\Psi|$ one has to increase the effective coupling, *i.e.*, go to higher values of $|F_j|$.

3.2 Mixed colorless vectorlike fermions

Let us now consider the case in which the colorless vectorlike fermions transform in different $SU(2)_L \times U(1)_Y$ representations, such that an invariant Yukawa coupling with the Higgs boson is allowed. Since a general discussion would be quite involved, we will consider two examples to illustrate the impact of the future experiments measuring the TGCs. Specifically, we will examine the two models studied in Ref. [38], corresponding to the addition of a singlet and a doublet, and a doublet plus a triplet of fermions.

Doublet-singlet model. We introduce a singlet Dirac fermion $N = N_L + N_R$ with hypercharge Y and a doublet Dirac fermion $L = L_L + L_R$ with hypercharge $Y - \frac{1}{2}$.² We will write explicitly the components of the L doublet as $L = (N_0, E)^T$ for the two chiralities. The Lagrangian is given by

$$\mathcal{L}_{2+1} = i\bar{L}\not{D}L + i\bar{N}\not{D}N - M_N\bar{N}_R N_L - M_L\bar{L}_R L_L - c\bar{N}_R H L_L - c'\bar{N}_L H L_R + h.c. \quad (3.3)$$

With the hypercharge assignment we are considering, the electric charges of the various components are

$$\begin{aligned} E &\rightarrow q_\chi \equiv Y - 1, \\ N, N_0 &\rightarrow q_\omega \equiv Y \end{aligned} \quad (3.4)$$

so that after electroweak symmetry breaking the Higgs introduces a mixing between N_0 and N , while E does not mix.

The three mass eigenstates $\omega_{1,2}$ and χ are defined as

$$\omega = \begin{pmatrix} \omega_1 \\ \omega_2 \end{pmatrix} = U_L^\dagger \begin{pmatrix} N \\ N_0 \end{pmatrix}_L + U_R^\dagger \begin{pmatrix} N \\ N_0 \end{pmatrix}_R, \quad \chi = E_L + E_R, \quad (3.5)$$

with $U_{L/R}$ the unitary matrices that diagonalize the mass matrix obtained from Eq. (3.3) after electroweak symmetry breaking.

In terms of the mass eigenstates, the gauge Lagrangian can be written as

$$\begin{aligned} \mathcal{L}_{\text{gauge}}^{2+1} = & e q_\chi \bar{\chi} \gamma^\mu \chi A_\mu + e q_\omega \bar{\omega} \gamma^\mu \omega A_\mu - \frac{1}{2} \left((2Y - 1) g' s_W + g c_W \right) \bar{\chi} \gamma^\mu \chi Z_\mu \\ & + \bar{\omega} \left[U_L^\dagger \begin{pmatrix} -Y g' s_W & 0 \\ 0 & \frac{1}{2} (g c_W - (2Y - 1) g' s_W) \end{pmatrix} U_L P_L + (L \rightarrow R) \right] \gamma^\mu \omega Z_\mu, \quad (3.6) \\ & + \frac{g}{\sqrt{2}} \bar{\omega} \gamma^\mu [U_L^\dagger P_L + U_R^\dagger P_R] (0 \quad W_\mu^+)^T \chi, \end{aligned}$$

where g and g' are the usual SM gauge couplings, $s_W = \sin \theta_W$ and $c_W = \cos \theta_W$.

²Notice that, although we use a notation suggesting heavier copies of a lepton doublet and right-handed neutrinos, we leave the hypercharge Y of N unspecified. The case $Y = 0$ corresponds, for example, to the situation studied in Ref. [13].

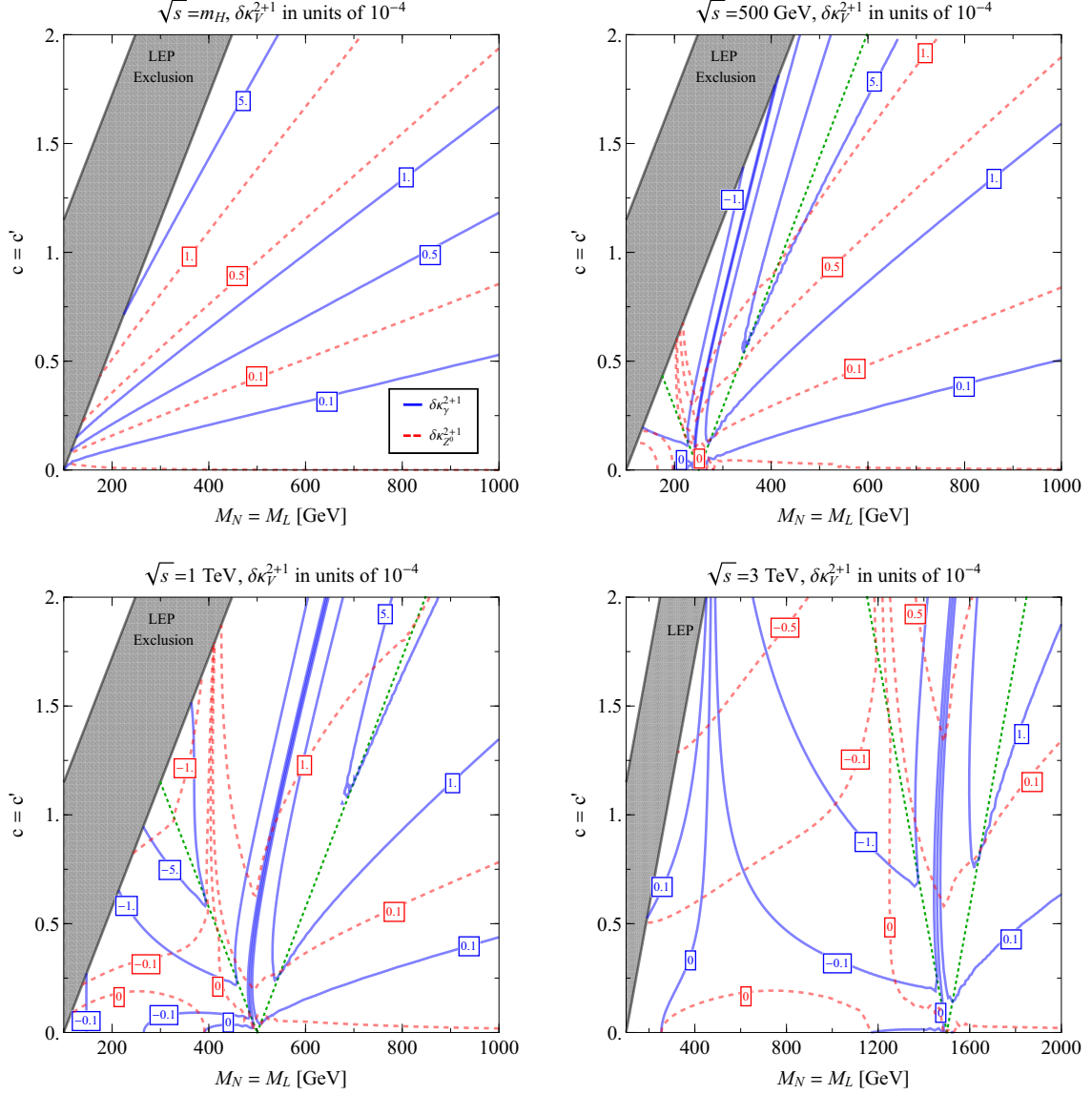


Figure 3. Isocontour lines of the deviations $\delta\kappa_V^{2+1}$ from the SM couplings in the plane ($M_N = M_L, c = c'$) for the vectorlike colorless fermion doublet-singlet model at four different center-of-mass energies: $\sqrt{s} = m_H, 500 \text{ GeV}, 1 \text{ TeV},$ and 3 TeV . We have chosen $Y = 1$, so ω_1 and ω_2 are charged, whereas χ is neutral. The full blue (dashed red) lines correspond to $V = \gamma$ (Z^0). The dotted green lines correspond to the physical masses m_{ω_1} and m_{ω_2} , for $M_N = M_L = \sqrt{s}/2$.

Having established our model, we proceed to compute the one-loop contributions of the new vectorlike fermions to the TGCs. Using the general result for the one-loop contribution, given in Appendix A, we compute the $\Delta\kappa_V^{2+1}$ and ΔQ_V^{2+1} form factors for this model. Note that the $W^+W^-Z^0$ vertex gets an additional correction with respect to the $W^+W^-\gamma$ one, due to the mixing between the doublet and the singlet.

In Fig. 3, we show the contour lines for $\delta\kappa_V^{2+1}$ in the (M, c) plane, where $M = M_L = M_N$ and $c' = c$, for the same four center-of-mass energies as before. Assuming c real, the

mass spectrum is $m_\chi = M$, $m_{\omega_1, \omega_2} = |M \pm 2cv|$, where $v = 175$ GeV is the SM Higgs vacuum expectation value. For an illustration, we have chosen the case $Y = 1$, so ω_1 and ω_2 are particles with charge 1 that participate in both $\delta\kappa_\gamma^{2+1}$ and $\delta\kappa_{Z^0}^{2+1}$, whereas χ is a neutral fermion and so it only contributes to the latter. For a fixed coupling $c = c'$, $\delta\kappa_\gamma^{2+1}$ has the following behavior as a function of $M = M_L = M_N$. It starts positive when, for a given center-of-mass energy, all vectorlike fermion masses are irrelevant for the loop function. Then, it decreases as the lowest fermion mass starts to play a role, until it reaches a minimum at $m_{\omega_1} = |\sqrt{s}/2 - 2cv|$; next, it increases when the next massive vectorlike fermion starts to contribute and passes again through zero before reaching a maximum at $m_{\omega_2} = \sqrt{s}/2 + 2cv$. As M_N continues to increase, $\delta\kappa_\gamma^{2+1} \rightarrow 0$ as we approach the decoupling limit. The behavior of $\delta\kappa_{Z^0}^{2+1}$ is somewhat similar but a bit more involved at lower values of M_N due to the mixing between $\omega_{1,2}$. Also, as M_N increases, the contribution of the neutral vectorlike fermion, χ , appears, giving rise to the maximum value for $\delta\kappa_{Z^0}^{2+1}$ at $M_N = m_\chi$. Here, again, the typical values of $|\delta\kappa_V^{2+1}|$ are smaller than a few 10^{-4} . The green dotted lines that can be seen on the $\sqrt{s} = 500$ GeV and 1 TeV panels correspond to the values of m_{ω_1} and m_{ω_2} computed with $M = \sqrt{s}/2$. At the other center-of-mass energies, these masses lie outside of the plot range.

Triplet-doublet model. We will now add to the SM particle content a Dirac $SU(2)_L$ doublet $L = L_L + L_R$ and a Dirac triplet $T = T_L + T_R$, with hypercharges Y and $Y - \frac{1}{2}$, respectively. The total Lagrangian is given by

$$\mathcal{L}_{3+2} = i\bar{L}\not{D}L + i\bar{T}\not{D}T - M_L\bar{L}_L L_R - M_T\bar{T}_L T_R - c\bar{L}_L T_R H - c'\bar{L}_R T_L H + h.c., \quad (3.7)$$

where the doublet and triplet fermions are written as

$$L = \begin{pmatrix} N_0 \\ E \end{pmatrix}, \quad T = \begin{pmatrix} \frac{T_a}{\sqrt{2}} & T_b \\ T_c & -\frac{T_a}{\sqrt{2}} \end{pmatrix}. \quad (3.8)$$

With the hypercharge assignment we are considering, the electric charges of the various components read

$$\begin{aligned} T_c &\rightarrow q_\chi \equiv Y - \frac{3}{2}, \\ T_a, E &\rightarrow q_\xi \equiv Y - \frac{1}{2}, \\ T_b, N_0 &\rightarrow q_\omega \equiv Y + \frac{1}{2}, \end{aligned} \quad (3.9)$$

in such a way that, after electroweak symmetry breaking, there is a mixing between T_a and E , as well as between T_b and N_0 . Defining the mass eigenstates as

$$\omega = \begin{pmatrix} \omega_1 \\ \omega_2 \end{pmatrix} = U_L^\dagger \begin{pmatrix} N_0 \\ T_b \end{pmatrix}_L + U_R^\dagger \begin{pmatrix} N_0 \\ T_b \end{pmatrix}_R, \quad \xi = \begin{pmatrix} \xi_1 \\ \xi_2 \end{pmatrix} = V_L^\dagger \begin{pmatrix} E \\ T_a \end{pmatrix}_L + V_R^\dagger \begin{pmatrix} E \\ T_a \end{pmatrix}_R, \quad (3.10)$$

$$\chi = T_{cL} + T_{cR},$$

the gauge Lagrangian can be written as

$$\begin{aligned}
\mathcal{L}_{3+2} = & e q_\chi \bar{\chi} \gamma^\mu \chi A_\mu + e q_\omega \bar{\omega} \gamma^\mu \omega A_\mu + e q_\xi \bar{\xi} \gamma^\mu \xi A_\mu - (q_\xi g' s_W + g c_W) \bar{\chi} \gamma^\mu \chi Z_\mu \\
& + \bar{\omega} \left[U_L^\dagger \begin{pmatrix} \frac{g}{2} c_W - Y g' s_W & 0 \\ 0 & g c_W - q_\xi g' s_W \end{pmatrix} U_L P_L + (L \rightarrow R) \right] \gamma^\mu \omega Z_\mu \\
& + \bar{\xi} \left[V_L^\dagger \begin{pmatrix} -\frac{g}{2} c_W - Y g' s_W & 0 \\ 0 & -q_\xi g' s_W \end{pmatrix} V_L P_L + (L \rightarrow R) \right] \gamma^\mu \xi Z_\mu \\
& + g (\bar{\omega} \ \bar{\xi} \ \bar{\chi}) \gamma^\mu \left[\begin{pmatrix} 0_{2 \times 2} & W_\mu^+ U_L^\dagger V_L' & 0_{2 \times 1} \\ W_\mu^- V_L'^\dagger U_L & 0_{2 \times 2} & V_L^\dagger \widetilde{W}_\mu^{+T} \\ 0_{1 \times 2} & \widetilde{W}_\mu^{-T} V_L & 0 \end{pmatrix} P_L + (L \rightarrow R) \right] \begin{pmatrix} \omega \\ \xi \\ \chi \end{pmatrix}, \quad (3.11)
\end{aligned}$$

where $\widetilde{W}_\mu^\pm = (0 \ W_\mu^\pm)$ and

$$V_L' = \frac{1}{\sqrt{2}} \begin{pmatrix} V_{L11} & V_{L12} \\ \sqrt{2} V_{L21} & \sqrt{2} V_{L22} \end{pmatrix}.$$

In Fig. 4, we show the isocontour lines for the $\delta\kappa_V^{3+2}$ combinations for this model in the plane $M_L = M_T$ vs $c = c'$ for the same four different center-of-mass energies as before. In this case the physical mass spectrum is $m_\chi = \sqrt{s}/2$, $m_{\omega_1} = |\sqrt{s}/2 - 2cv|$, $m_{\omega_2} = \sqrt{s}/2 + 2cv$, $m_{\xi_1} = |\sqrt{s}/2 - \sqrt{2}cv|$, and $m_{\xi_2} = \sqrt{s}/2 + \sqrt{2}cv$. The green dotted lines that can be seen on the $\sqrt{s} = 500$ GeV and 1 TeV panels correspond to the values of the charged particle masses m_{ω_1} , m_{ω_2} , and m_χ . At the other center-of-mass energies these masses lie outside of the plot range.

Here, we show the case $Y = 1/2$, so χ , ω_1 , and ω_2 are charged particles that participate of both $\delta\kappa_\gamma^{3+2}$ and $\delta\kappa_{Z^0}^{3+2}$, whereas ξ_1 and ξ_2 are neutral fermions and only contribute to the latter. Here, the typical values of $|\delta\kappa_V^{3+2}|$ can get about an order of magnitude larger than in the previous models, but the form factors are always smaller than a few 10^{-3} .

For a fixed coupling c , $\delta\kappa_\gamma^{3+2}$ as a function of M_L has the same general behavior as for the doublet-singlet model. It goes through a minimum at m_{ω_1} , and through a maximum at m_χ and m_{ω_2} . This can be best seen on the panel for $\sqrt{s} = 1$ TeV. The behavior of $\delta\kappa_{Z^0}^{3+2}$ is somewhat similar but even more involved than the previous mixed case because now we have five particles coupling to the Z^0 so in addition to the charged particle peaks, we also have peaks for the neutral particles. We note that in this case $|\delta\kappa_{Z^0}^{3+2}| \sim |\delta\kappa_\gamma^{3+2}|$ and sometimes even a bit larger.

4 TGC constraints on vectorlike colorless fermion models

We move now to estimate the possible future constraints that can be imposed on vectorlike colorless fermion models by TGC measurements at future e^+e^- accelerator facilities such as the proposed FCC-ee [27], ILC [28], and the CLIC [29]. For the FCC-ee experiment we

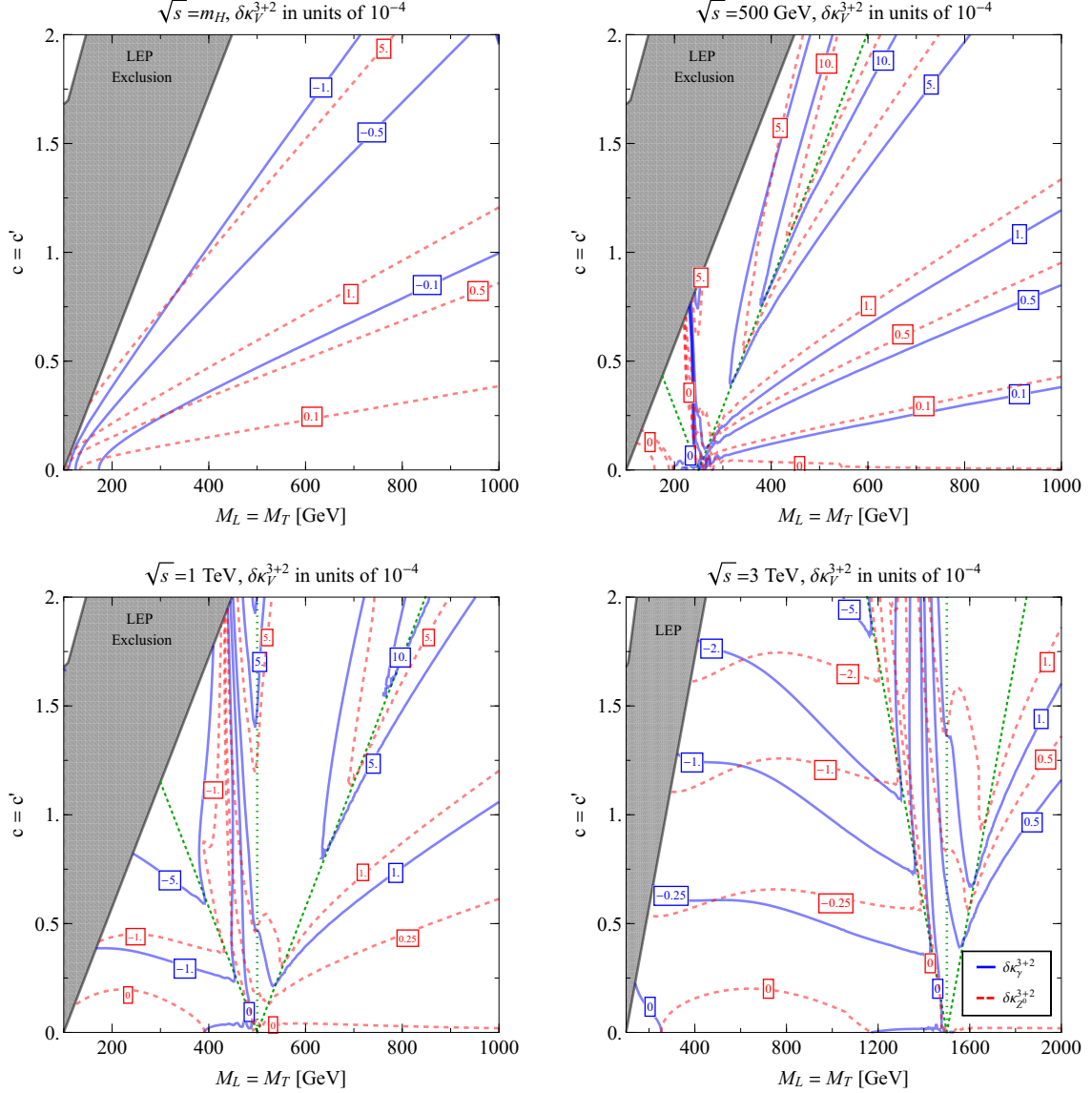


Figure 4. Isocontour lines of the deviations $\delta\kappa_V^{3+2}$ from the SM couplings in the plane $(M_L = M_T, c = c')$ for the vectorlike colorless fermion triplet-doublet model at four different center-of-mass energies: $\sqrt{s} = m_H$, 500 GeV, 1 TeV, and 3 TeV. We have chosen $Y = 1/2$, so there are three charged states and two neutral ones. The full blue (dashed red) lines correspond to $V = \gamma$ (Z^0), and the dotted green lines correspond to the physical masses m_{ω_1} , m_{ω_2} , and m_χ .

considered the following center-of-mass energies: $\sqrt{s} = m_Z$, m_H , $2m_Z$ and $2m_t$ [27], for the ILC: $\sqrt{s} = 500$, 800, and 1000 GeV [28]; and for the CLIC (in the so-called scenario A): $\sqrt{s} = 500$, 1400, and 3000 GeV [29].

We do this for each of the models addressed in this paper by minimizing a combined $\chi^2(\delta\kappa_Z, \delta\kappa_\gamma; \sqrt{s}_i)$ assuming the following three different benchmark sensitivities for both TGCs: 4×10^{-4} , 2×10^{-4} , and 1×10^{-4} [39, 40]. We assume the same benchmarks for all facilities at all center-of-mass energies.

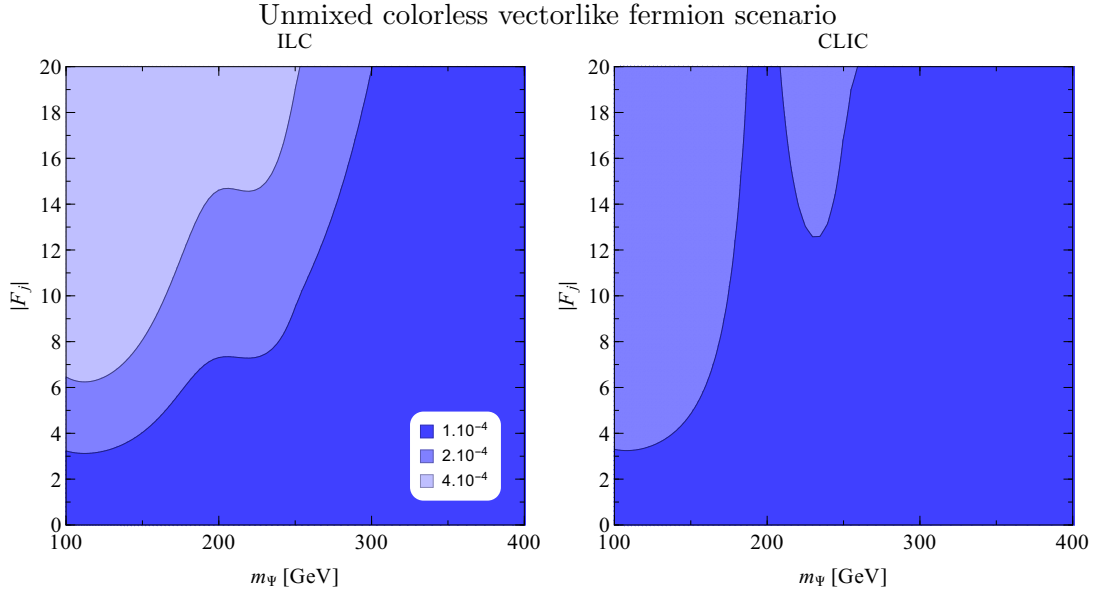


Figure 5. Possible TGC reach to probe the parameters of the unmixed vectorlike colorless fermion models by combining different center-of-mass energies at the ILC ($\sqrt{s} = 500, 800, 1000$ GeV) and the CLIC ($\sqrt{s} = 500, 1400, 3000$ GeV) facilities. We assume the same three different sensitivities for $\delta\kappa_\gamma$ and $\delta\kappa_{Z^0}$ at all center-of-mass energies considered: 4×10^{-4} , 2×10^{-4} and 1×10^{-4} . The regions of accessibility were computed at 95.45% C.L.. See the text for more details.

In Fig. 5, we show the regions on the plane $(m_\Psi, |F_j|)$ of the unmixed vectorlike model that can be probed at 2σ C.L. by combining the various center-of-mass energies at these accelerators. Because of the relatively low center-of-mass energies proposed for the FCC-ee, it can only probe a very limited range of $m_\Psi \lesssim 200$ GeV for $|F_j| \gtrsim (1 - 4)$ at 2σ C.L. if the sensitivity is at least 1×10^{-4} . This is why we do not show this case on Fig. 5. The ILC will be able to test $m_\Psi \lesssim 250$ GeV ($m_\Psi \lesssim 300$ GeV) for $|F_j| \gtrsim 16$ if a sensitivity of 2×10^{-4} (1×10^{-4}) can be achieved. At the CLIC, the reach is somewhat reduced, as, for instance, no region is accessible at 2σ C.L. even for a sensitivity of 2×10^{-4} for $|F_j| < 20$. Note that the CLIC is less sensitive to the unmixed colorless vectorlike scenario than the ILC due to its higher center-of-mass energies as explained by the following reasoning. As can be seen in Fig. 2, the contribution to TGCs is higher when \sqrt{s} is close to the vectorlike fermions mass threshold, but the heavier the fermions are, the smaller the TGC deviation is in general. Deviations at the $\mathcal{O}(10^{-4})$ level are typically caused by particles below the TeV scale, and thus having a lower center-of-mass energy leads to better sensitivity.

In Fig. 6, we show the regions on the plane $(M_N = M_L, c = c')$ of the doublet-singlet model with $Y = 1$ that can be explored by the FCC-ee, ILC, and CLIC at 2σ C.L.. This is performed as before, that is, by combining the χ^2 at the center-of-mass energies of each facility. For comparison, we also show the current limits one can obtain from $H \rightarrow \gamma\gamma$ ($R_{\gamma\gamma}$, full red line; see, e.g., Ref. [41]) and electroweak precision measurements (δT , full dark green line) as well as the effect of a future possible improvement on the uncertainty on $R_{\gamma\gamma}$ to 8% (dashed red line) or 3% (dotted-dashed red line) and on the uncertainty

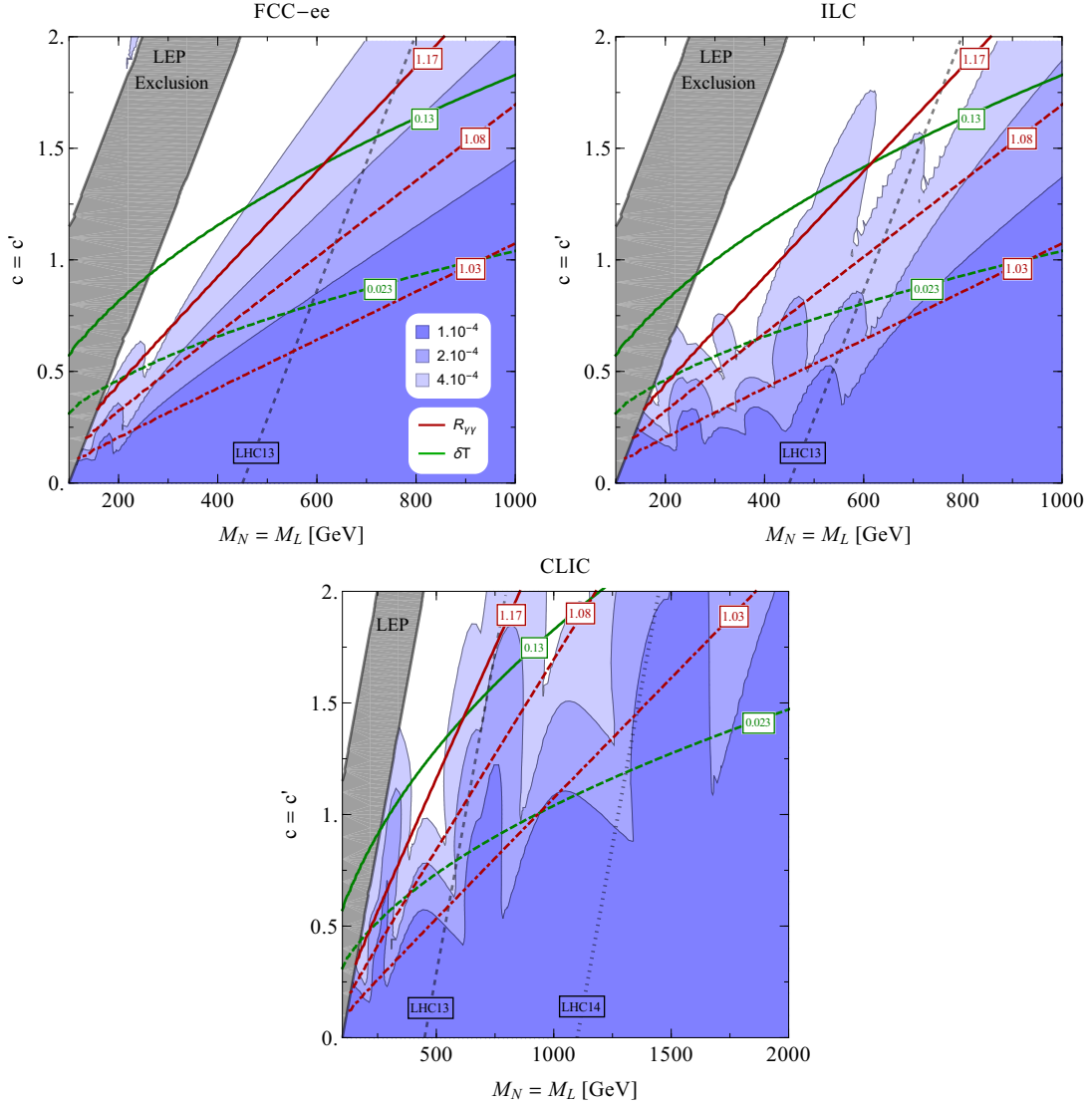


Figure 6. Possible TGC reach to probe the parameters of the doublet-singlet vectorlike colorless fermion model with $Y = 1$, by combining different center-of-mass energies at the FCC-ee, the ILC and the CLIC facilities at 2σ C.L.. We also show the current limits from $H \rightarrow \gamma\gamma$ ($R_{\gamma\gamma}$, full red line) and electroweak precision measurements (δT , full dark green line) as well as the possible future sensitivities of $R_{\gamma\gamma}$ assuming an uncertainty of 8% (dashed red line) or 3% (dotted-dashed red line) and of δT (dashed dark green line). The gray region has been excluded by LEP [24], while the black dashed (dotted) lines correspond to the LHC current limit (future sensitivity).

on δT (dashed dark green line). These future prospects on the uncertainties were taken from Refs. [28, 42]; for comparison we show the same δT and $R_{\gamma\gamma}$ sensitivities for all proposed facilities. The region in gray was excluded by LEP searches for neutral and charged leptons [24].

At present, $R_{\gamma\gamma}$ excludes more of the parameter space of the doublet-singlet model than δT if $M_N \lesssim 600$ GeV, but for larger values of M_N , δT is more restrictive. We see that at the

FCC-ee one can have the sensitivity to probe and exclude a larger region of the parameter space, which can only be comparable to a future sensitivity on $R_{\gamma\gamma}$ of 8% or better, if one can reach a sensitivity of $\sim 1.5 \times 10^{-4}$ on the TGCs. Here since the center-of-mass energies that we have combined are comparatively low, the peak structure only appears around $M_N \sim 180$ GeV, the rest of the exclusion region being quite smooth. At the ILC, because the center-of-mass energies are higher, the exclusion region is more complicated due to the maxima and minima that appear for the different masses of the vectorlike fermions that run in the loop functions at different \sqrt{s} . In general, the ILC can exclude the same regions probed by the FCC-ee but, most of the parameter space, requiring a less challenging sensitivity to the TGCs.

Although the CLIC involves even higher center-of-mass energies, it loses some sensitivity for $M_N \sim 700$ GeV because of the peaks structure. Nevertheless, it can test the regions $800 \lesssim M_N/\text{GeV} \lesssim 1400$ and $1600 \lesssim M_N/\text{GeV} \lesssim 1900$ for a TGC sensitivity of 1×10^{-4} . Such region could only be inspected by a $R_{\gamma\gamma}$ or a δT measurement with 2%-3% uncertainty.

Finally, in Fig. 7 we show the regions on the plane ($M_L = M_T, c = c'$) of the triplet-doublet model with $Y = 1/2$ that can be explored at 2σ C.L. by the FCC-ee, ILC, and CLIC, again combining the same center-of-mass energies as before. In this case, the FCC-ee can explore a region than can only be attainable by measuring $R_{\gamma\gamma}$ with an uncertainty of at least 3% if the TGC sensitivity is 2×10^{-4} , while the ILC is a bit better except for $M_L \lesssim 250$ GeV. As before CLIC is, in general, less sensitive for $M_L \lesssim 700$ GeV because of the peak structure but becomes more sensitive for higher masses, probing the model down to regions where even a very aggressive measurement of $R_{\gamma\gamma}$ would not reach.

Let us conclude with some remarks about the limits from direct searches at the LHC. As shown, for instance, in Refs. [13, 43], the collider signatures of the doublet-singlet model are very similar to those of electroweakinos in minimal supersymmetry models. Moreover, we expect the limits for the other representations not to be too different. Current lower bounds can be found in Ref. [44] and are of order 150 GeV for the lightest neutral state and of order 450 GeV for the heavier states. Future sensitivities have been estimated in Ref. [45]; with a luminosity of 3000 fb^{-1} (at $\sqrt{s} = 14$ TeV), the lower bound on the lightest neutral mass becomes 400 GeV, while the lower bound on the heavier states becomes 1.1 TeV. We included the current limit (dashed black line) and future sensitivity (dotted black line) in Figs. 6 and 7. As can be seen, even considering the future LHC reach, there are regions not probed by the LHC that will be probed by TGCs searches.

5 Conclusions

We have studied vectorlike colorless fermions contributions to the triple gauge couplings $W^+W^-\gamma$ and $W^+W^-Z^0$ in the context of two classes of models. First, we considered the unmixed case, in which an arbitrary set of fermions in a given representation of $SU(2)_L$ cannot couple to the SM Higgs boson. Second, we considered the mixed case, where

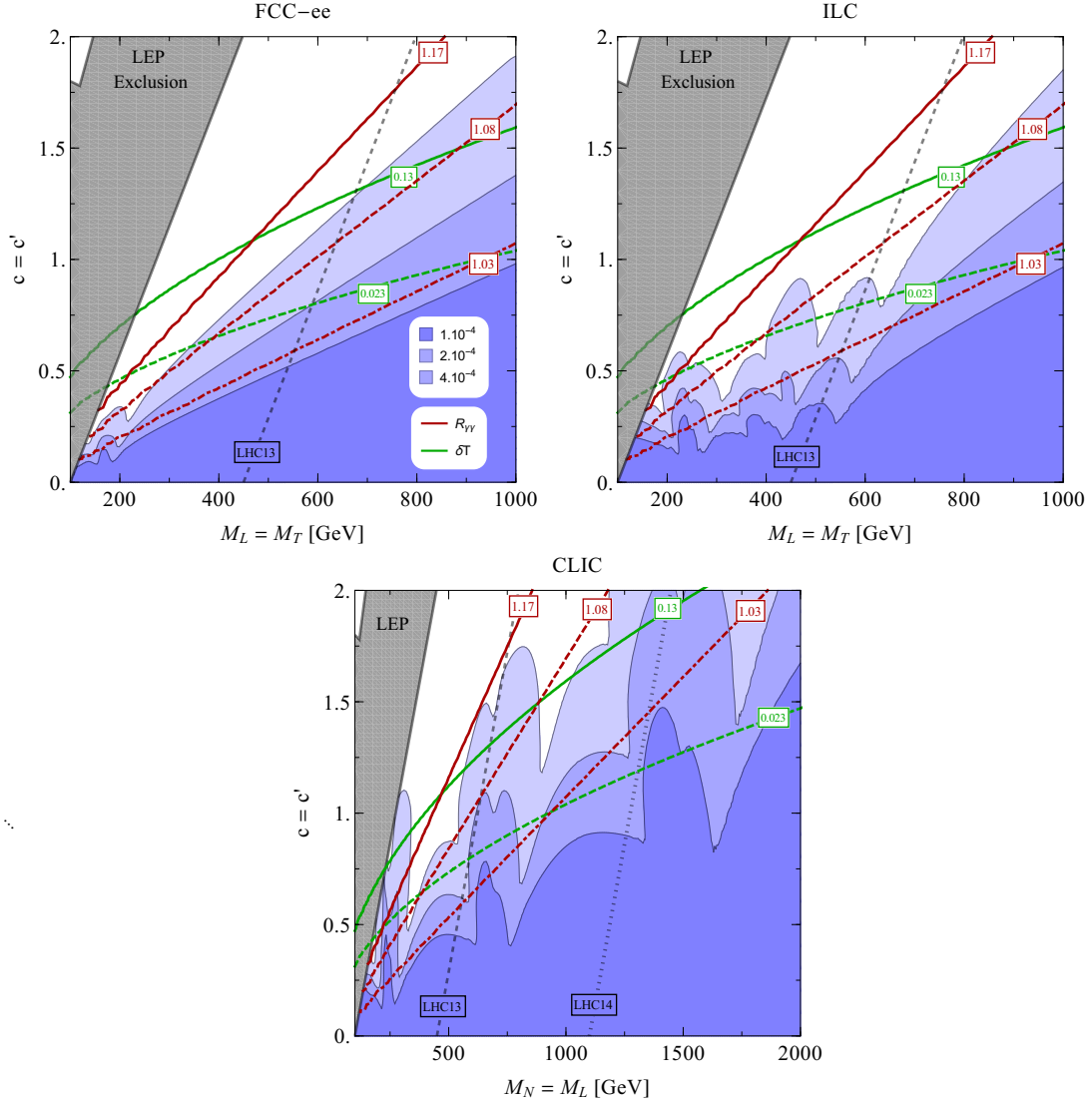


Figure 7. Same as Fig. 6 but for the triplet-doublet vectorlike colorless fermion model with $Y = 1/2$.

the vectorlike fermion fields transform as different representations of $SU(2)_L$ allowing for invariant Yukawa couplings with the Higgs boson. In the latter case, we studied two concrete situations: the doublet-singlet model, where three new vectorlike physical particles are introduced, and the triplet-doublet model, where five new vectorlike physical particles appear.

We established that the contributions of the above vectorlike fermion models to the combination of the form factors, $\delta\kappa_V$, $V = \gamma, Z^0$, used by the experimental collaborations, have several minima and maxima as a function of the mass parameters of the model. Since to go from a negative minimum to a positive maximum one has to cross zero, this also implies that there are values of the mass parameter for which $\delta\kappa_V \rightarrow 0$. These maxima

and minima will depend on the center-of-mass energy considered, and how close one is to a physical particle which contributes to the TGC loop function being on the mass shell.

In the case of the unmixed vectorlike colorless fermion model, we have assumed that all fermions, independent of how many multiplets of a given representation, are degenerate in mass (m_Ψ). Since $|\delta\kappa_\gamma|$ starts large when $m_\Psi \ll \sqrt{s}/2$, and we expect a maximum at $m_\Psi \sim \sqrt{s}/2$, there are, in general, two values of m_Ψ , for a given \sqrt{s} , where $\delta\kappa_V \rightarrow 0$.

For the doublet-singlet and triplet-doublet model the minima and maxima for $\delta\kappa_\gamma$ ($\delta\kappa_{Z^0}$) as a function of M_L , the mass parameter, correspond to the values of the charged (all) physical particles of the model, which clearly depend on \sqrt{s} and the hypercharge Y , which defines the charges of the particles.

We made an assessment of the sensitivity of the proposed future precision test accelerators, the FCC-ee, ILC, and CLIC to the parameters of these models assuming they will be able to constrain $\delta\kappa_V \sim \mathcal{O}(10^{-4})$ at different \sqrt{s} . Using the same benchmark sensitivities for all accelerators allowed us to clearly see the effect of the different center-of-mass energy combinations. For the FCC-ee experiment we considered the following center-of-mass energies: $\sqrt{s} = m_Z, m_H, 2m_Z$ and $2m_t$. For the ILC: $\sqrt{s} = 500, 800, \text{ and } 1000$ GeV, and for the CLIC (in the so-called scenario A): $\sqrt{s} = 500, 1400, \text{ and } 3000$ GeV.

Only for the unmixed vectorlike colorless fermion case, the FCC-ee is definitely not as capable to probe the model as the ILC or the CLIC. However, for both mixed vectorlike models we have examined, the ILC is generally better than the FCC-ee but not as powerful as the CLIC at larger values of the mass parameters M_N or M_L . This is because the \sqrt{s} used by FCC-ee are all quite low, making the exclusion region basically insensitive to the maxima and minima caused by the physical particle masses. For the ILC, the gaps between the center-of-mass energies and their high values exhibit some synergy that helps to improve the sensitivity in a large region of the parameter. This also happens for the CLIC, but since the center-of-mass energies are more spread out, there is an overall decrease in sensitivity to the model parameters for $M_N, M_L \lesssim 700$ GeV, with respect to the ILC. However, for higher masses (due to the 3000 GeV center-of-mass energy contribution) we have again an increase of sensitivity because heavier vectorlike fermion physical masses come into play.

It is also important to note that if one is able to achieve $\mathcal{O}(10^{-4})$ sensitivity on TGCs with the FCC-ee, ILC, or CLIC one will be able to use them to do precision measurements that surpass the sensitivities of the oblique parameters or $H \rightarrow \gamma\gamma$ even assuming a considerable improvement of the latter measurements in these new machines.

Acknowledgments

P. M. thanks the Universidade de São Paulo for the kindest hospitality. This work was supported by Fundação de Amparo à Pesquisa do Estado de São Paulo (FAPESP) and Conselho Nacional de Ciência e Tecnologia (CNPq). This project has also received partial

funding from the European Union’s Horizon 2020 research and innovation program under the Marie Skłodowska-Curie Grants No. 674896 and No. 690575. Fermilab is operated by Fermi Research Alliance, LLC, under Contract No. DE-AC02-07CH11359 with the US Department of Energy.

A Vectorlike fermion contribution to triple gauge couplings

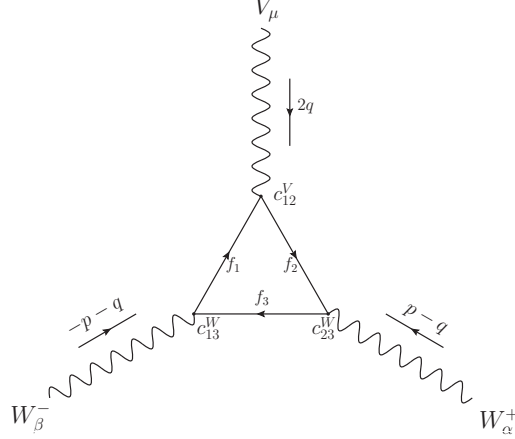


Figure 8. Vectorlike fermions contribution to TGC.

The one-loop correction to the TGCs coming from a set of N_F vectorlike fermions can be obtained from the diagram in Fig. 8. Here, we will keep as general as possible, by supposing that three different fermions run into the loop, f_i , $i = \{1, 2, 3\}$, with masses m_i and generic couplings between them and the gauge bosons, c_{ij}^B , where $i, j = \{1, 2, 3\}$ and $B = \{\gamma, W, Z\}$. Proceeding in a standard way, we find the $\Delta\kappa_V^{NP}$ and ΔQ_V^{NP} form factors,

$$\begin{aligned} \Delta\kappa_V^{NP} = -N_F \frac{c_{12}^V c_{23}^W c_{31}^W}{8\pi^2 g_V} \int_0^1 dx \int_0^1 dy \frac{x}{\tilde{\Lambda}} \left\{ \frac{4q^2}{M_W^2} x^2 (3x-2)y(1-y) + x^2(x-1) \right. \\ \left. + (R_1 - R_2)xy(x-1) + (R_3 - R_1)x(x-1) + \sqrt{R_1 R_2}x \right. \\ \left. + \sqrt{R_2 R_3}(1-x-2xy) + \sqrt{R_1 R_3}(1-3x+2xy) \right\}, \quad (\text{A.1a}) \end{aligned}$$

$$\Delta Q_V^{NP} = -N_F \frac{c_{12}^V c_{23}^W c_{31}^W}{\pi^2 g_V} \int_0^1 dx \int_0^1 dy \frac{x^3(1-x)y(1-y)}{\tilde{\Lambda}}, \quad (\text{A.1b})$$

where

$$\tilde{\Lambda} = -\frac{4q^2}{M_W^2} x^2 y(1-y) + x^2 - x(1 + R_3 - R_1) - (R_1 - R_2)xy + R_3, \quad (\text{A.2})$$

and $R_i = \frac{m_i^2}{M_W^2}$.

to determine the form factors $\Delta\kappa_V^\Psi$ and ΔQ_V^Ψ . Each diagram can be written as a product of the couplings of the fermions with the gauge bosons times a loop integral, $I_{\mu\alpha\beta}(m_m, m_m, m_{m\pm 1})$. Therefore, the amplitude will be

$$\Gamma_{\mu\alpha\beta}^V = \frac{g^2}{4} \sum_{m=-j}^j g_V^m [(j+1-m)(j+m)I_{\mu\alpha\beta}(m_m, m_m, m_{m-1}) + (j-m)(j+m+1)I_{\mu\alpha\beta}(m_m, m_m, m_{m+1})], \quad (\text{B.5})$$

where

$$g_V^m = \begin{cases} e(m+Y) & \text{for } \gamma, \\ \frac{g}{c_W}(c_W^2 m - s_W^2 Y) & \text{for } Z^0. \end{cases} \quad (\text{B.6})$$

Since the mass of the components of the multiplet is the same, we have that the loop integral will depend only on the mass m_Ψ ,

$$I_{\mu\alpha\beta}(m_m, m_m, m_{m\pm 1}) = I_{\mu\alpha\beta}(m_\Psi),$$

then, the amplitude will take a simpler form,

$$\Gamma_{\mu\alpha\beta}^V = \frac{g^2}{2} I_{\mu\alpha\beta}(m_\Psi) \sum_{m=-j}^j g_V^m [j(j+1) - m^2]. \quad (\text{B.7})$$

Summing over the magnetic quantum number m ,

$$\sum_{m=-j}^j [j(j+1) - m^2] = \frac{2}{3} j(j+1)(2j+1), \quad (\text{B.8a})$$

$$\sum_{m=-j}^j m[j(j+1) - m^2] = 0, \quad (\text{B.8b})$$

we see here that the amplitude of the one-loop correction will be proportional to the hypercharge,

$$\Gamma_{\mu\alpha\beta}^V = \frac{g^2 c_\Psi^V Y}{3} j(j+1)(2j+1) I_{\mu\alpha\beta}(m_\Psi), \quad (\text{B.9})$$

being

$$c_\Psi^V = \begin{cases} e & \text{for } \gamma, \\ -e t_W & \text{for } Z^0, \end{cases} \quad (\text{B.10})$$

with $t_W = \tan\theta_W$. Finally, the form factors will be computed in a standard manner. The expressions for $\Delta\kappa_V^\Psi$ and ΔQ_V^Ψ can be obtained from the general expressions in Appendix A by taking all the masses as identical and

$$c_{23}^W = c_{13}^W = \frac{g}{\sqrt{2}} G_j, \quad (\text{B.11})$$

$$c_{12}^V = c_\Psi^V Y, \quad (\text{B.12})$$

where G_j is the square root of the multiplet factor,

$$G_j = \sqrt{\frac{2}{3} j(j+1)(2j+1)}. \quad (\text{B.13})$$

References

- [1] C. Kilic, T. Okui, and R. Sundrum, *Vectorlike Confinement at the LHC*, JHEP **02** (2010) 018, [[arXiv:0906.0577](#)].
- [2] P. H. Frampton, P. Q. Hung, and M. Sher, *Quarks and leptons beyond the third generation*, Phys. Rept. **330** (2000) 263, [[hep-ph/9903387](#)].
- [3] K. Agashe, T. Okui, and R. Sundrum, *A Common Origin for Neutrino Anarchy and Charged Hierarchies*, Phys. Rev. Lett. **102** (2009) 101801, [[arXiv:0810.1277](#)].
- [4] S. Gopalakrishna, T. Mandal, S. Mitra, and G. Moreau, *LHC Signatures of Warped-space Vectorlike Quarks*, JHEP **08** (2014) 079, [[arXiv:1306.2656](#)].
- [5] S. Fichtel and G. von Gersdorff, *Anomalous gauge couplings from composite Higgs and warped extra dimensions*, JHEP **03** (2014) 102, [[arXiv:1311.6815](#)].
- [6] D. B. Kaplan, *Flavor at SSC energies: A New mechanism for dynamically generated fermion masses*, Nucl. Phys. **B365** (1991) 259–278.
- [7] M. Redi, *Leptons in Composite MFV*, JHEP **09** (2013) 060, [[arXiv:1306.1525](#)].
- [8] R. Contino and A. Pomarol, *Holography for fermions*, JHEP **11** (2004) 058, [[hep-th/0406257](#)].
- [9] R. Dermisek, E. Lunghi, and S. Shin, *Two Higgs doublet model with vectorlike leptons and contributions to $pp \rightarrow WW$ and $H \rightarrow WW$* , JHEP **02** (2016) 119, [[arXiv:1509.04292](#)].
- [10] S. P. Martin, *Extra vector-like matter and the lightest Higgs scalar boson mass in low-energy supersymmetry*, Phys. Rev. **D81** (2010) 035004, [[arXiv:0910.2732](#)].
- [11] P. W. Graham, A. Ismail, S. Rajendran, and P. Saraswat, *A Little Solution to the Little Hierarchy Problem: A Vector-like Generation*, Phys. Rev. **D81** (2010) 055016, [[arXiv:0910.3020](#)].
- [12] P. W. Graham, D. E. Kaplan, and S. Rajendran, *Cosmological Relaxation of the Electroweak Scale*, Phys. Rev. Lett. **115** (2015), no. 22 221801, [[arXiv:1504.07551](#)].
- [13] A. Arvanitaki, S. Dimopoulos, V. Gorbenko, J. Huang, and K. Van Tilburg, *A small weak scale from a small cosmological constant*, [arXiv:1609.06320](#).
- [14] C. Anastasiou, S. Buehler, E. Furlan, F. Herzog, and A. Lazopoulos, *Higgs production cross-section in a Standard Model with four generations at the LHC*, Phys. Lett. **B702** (2011) 224–227, [[arXiv:1103.3645](#)].
- [15] C. Anastasiou, C. Duhr, F. Dulat, E. Furlan, T. Gehrmann, F. Herzog, A. Lazopoulos, and B. Mistlberger, *High precision determination of the gluon fusion Higgs boson cross-section at the LHC*, JHEP **05** (2016) 058, [[arXiv:1602.00695](#)].
- [16] CMS Collaboration, S. Chatrchyan et al., *Inclusive search for a vector-like T quark with charge $\frac{2}{3}$ in pp collisions at $\sqrt{s} = 8$ TeV*, Phys. Lett. **B729** (2014) 149–171, [[arXiv:1311.7667](#)].
- [17] CMS Collaboration, S. Chatrchyan et al., *Search for top-quark partners with charge $5/3$ in the same-sign dilepton final state*, Phys. Rev. Lett. **112** (2014), no. 17 171801, [[arXiv:1312.2391](#)].
- [18] CMS Collaboration, V. Khachatryan et al., *Search for vector-like T quarks decaying to top quarks and Higgs bosons in the all-hadronic channel using jet substructure*, JHEP **06** (2015)

080, [[arXiv:1503.01952](#)].

- [19] **CMS** Collaboration, V. Khachatryan et al., *Search for pair-produced vectorlike B quarks in proton-proton collisions at $\sqrt{s} = 8$ TeV*, Phys. Rev. **D93** (2016), no. 11 112009, [[arXiv:1507.07129](#)].
- [20] **ATLAS** Collaboration, G. Aad et al., *Search for vector-like B quarks in events with one isolated lepton, missing transverse momentum and jets at $\sqrt{s} = 8$ TeV with the ATLAS detector*, Phys. Rev. **D91** (2015), no. 11 112011, [[arXiv:1503.05425](#)].
- [21] **ATLAS** Collaboration, G. Aad et al., *Search for production of vector-like quark pairs and of four top quarks in the lepton-plus-jets final state in pp collisions at $\sqrt{s} = 8$ TeV with the ATLAS detector*, JHEP **08** (2015) 105, [[arXiv:1505.04306](#)].
- [22] **ATLAS** Collaboration, G. Aad et al., *Search for the production of single vector-like and excited quarks in the Wt final state in pp collisions at $\sqrt{s} = 8$ TeV with the ATLAS detector*, JHEP **02** (2016) 110, [[arXiv:1510.02664](#)].
- [23] **ATLAS** Collaboration, G. Aad et al., *Search for single production of vector-like quarks decaying into Wb in pp collisions at $\sqrt{s} = 8$ TeV with the ATLAS detector*, Eur. Phys. J. **C76** (2016), no. 8 442, [[arXiv:1602.05606](#)].
- [24] **L3** Collaboration, P. Achard et al., *Search for heavy neutral and charged leptons in e^+e^- annihilation at LEP*, Phys. Lett. **B517** (2001) 75–85, [[hep-ex/0107015](#)].
- [25] W. Altmannshofer, M. Bauer, and M. Carena, *Exotic Leptons: Higgs, Flavor and Collider Phenomenology*, JHEP **01** (2014) 060, [[arXiv:1308.1987](#)].
- [26] C. Cai, Z.-H. Yu, and H.-H. Zhang, *CEPC Precision of Electroweak Oblique Parameters and Weakly Interacting Dark Matter: the Fermionic Case*, Nucl. Phys. **B921** (2017) 181–210, [[arXiv:1611.02186](#)].
- [27] D. d’Enterria, *Physics at the FCC-ee*, in Proceedings, 17th Lomonosov Conference on Elementary Particle Physics., pp. 182–191, World Scientific, 2017. [arXiv:1602.05043](#).
- [28] H. Baer, T. Barklow, K. Fujii, Y. Gao, A. Hoang, S. Kanemura, J. List, H. E. Logan, A. Nomerotski, M. Perelstein, et al., *The International Linear Collider Technical Design Report - Volume 2: Physics*, [arXiv:1306.6352](#).
- [29] D. Dannheim, P. Lebrun, L. Linssen, D. Schulte, F. Simon, S. Stapnes, N. Toge, H. Weerts, and J. Wells, *CLIC $e+e-$ Linear Collider Studies*, [arXiv:1208.1402](#).
- [30] E. N. Argyres, G. Katsilieris, A. B. Lahanas, C. G. Papadopoulos, and V. C. Spanos, *One loop corrections to three vector boson vertices in the Standard Model*, Nucl. Phys. **B391** (1993) 23–41.
- [31] J. Papavassiliou and K. Philippides, *Gauge invariant three boson vertices in the Standard Model and the static properties of the W* , Phys. Rev. **D48** (1993) 4255–4268, [[hep-ph/9310210](#)].
- [32] J. Fleischer, J. L. Kneur, K. Kolodziej, M. Kuroda, and D. Schildknecht, *One loop improved Born approximation for $e^+e^- \rightarrow W^+W^-$* , Nucl. Phys. **B378** (1992) 443–467. [Erratum: Nucl. Phys.B426,246(1994)].
- [33] G. J. Gounaris, J. Layssac, and F. M. Renard, *New and standard physics contributions to anomalous Z and gamma selfcouplings*, Phys. Rev. **D62** (2000) 073013, [[hep-ph/0003143](#)].

- [34] **CMS** Collaboration, V. Khachatryan et al., *Measurement of the $Z\gamma$ Production Cross Section in pp Collisions at 8 TeV and Search for Anomalous Triple Gauge Boson Couplings*, *JHEP* **04** (2015) 164, [[arXiv:1502.05664](#)].
- [35] **CMS** Collaboration, V. Khachatryan et al., *Measurements of the $Z Z$ production cross sections in the $2l2\nu$ channel in proton–proton collisions at $\sqrt{s} = 7$ and 8 TeV and combined constraints on triple gauge couplings*, *Eur. Phys. J.* **C75** (2015), no. 10 511, [[arXiv:1503.05467](#)].
- [36] **CMS** Collaboration, V. Khachatryan et al., *Measurement of the $Z\gamma \rightarrow \nu\bar{\nu}\gamma$ production cross section in pp collisions at $\sqrt{s} = 8$ TeV and limits on anomalous $ZZ\gamma$ and $Z\gamma\gamma$ trilinear gauge boson couplings*, *Phys. Lett.* **B760** (2016) 448–468, [[arXiv:1602.07152](#)].
- [37] K. Hagiwara, R. D. Peccei, D. Zeppenfeld, and K. Hikasa, *Probing the Weak Boson Sector in $e^+e^- \rightarrow W^+W^-$* , *Nucl. Phys.* **B282** (1987) 253–307.
- [38] L. G. Almeida, E. Bertuzzo, P. A. N. Machado, and R. Zukanovich Funchal, *Does $H \rightarrow \gamma\gamma$ Taste like vanilla New Physics?*, *JHEP* **11** (2012) 085, [[arXiv:1207.5254](#)].
- [39] J. Ellis and T. You, *Sensitivities of Prospective Future $e+e-$ Colliders to Decoupled New Physics*, *JHEP* **03** (2016) 089, [[arXiv:1510.04561](#)].
- [40] T. Barklow, J. Brau, K. Fujii, J. Gao, J. List, N. Walker, and K. Yokoya, *ILC Operating Scenarios*, [arXiv:1506.07830](#).
- [41] M. Carena, I. Low, and C. E. M. Wagner, *Implications of a Modified Higgs to Diphoton Decay Width*, *JHEP* **08** (2012) 060, [[arXiv:1206.1082](#)].
- [42] **Gfitter Group** Collaboration, M. Baak, J. Cúth, J. Haller, A. Hoecker, R. Kogler, K. Mönig, M. Schott, and J. Stelzer, *The global electroweak fit at NNLO and prospects for the LHC and ILC*, *Eur. Phys. J.* **C74** (2014) 3046, [[arXiv:1407.3792](#)].
- [43] H. Beauchesne, E. Bertuzzo, and G. Grilli di Cortona, *Constraints on the relaxion mechanism with strongly interacting vector-fermions*, [arXiv:1705.06325](#).
- [44] **CMS** Collaboration, A. M. Sirunyan et al., *Search for electroweak production of charginos and neutralinos in WH events in proton-proton collisions at $\sqrt{s} = 13$ TeV*, [arXiv:1706.09933](#).
- [45] **ATLAS** Collaboration, A. Collaboration, *Prospects for benchmark Supersymmetry searches at the high luminosity LHC with the ATLAS Detector*, .